Geophysical Research Letters

RESEARCH LETTER
10.1029/2023GL108039

Internal-Wave Dissipation Mechanisms and Vertical Structure in a High-Resolution Regional Ocean Model

Joseph Skitka[1,2], Brian K. Arbic[1], Yuchen Ma[3], Kayhan Momeni[3], Yulin Pan[4], William R. Peltier[3], Dimitris Menemenlis[5], and Ritabrata Thakur[1,6]

[1]Department of Earth and Environmental Sciences, University of Michigan, Ann Arbor, MI, USA, [2]Woods Hole Oceanographic Institution, Woods Hole, MA, USA, [3]Department of Physics, University of Toronto, Toronto, ON, Canada, [4]Department of Naval Architecture and Marine Engineering, University of Michigan, Ann Arbor, MI, USA, [5]Jet Propulsion Laboratory, California Institute of Technology, Pasadena, CA, USA, [6]Department of Applied Mechanics, Indian Institute of Technology Delhi, New Delhi, India

Abstract Motivated by the importance of mixing arising from dissipating internal waves (IWs), vertical profiles of internal-wave dissipation from a high-resolution regional ocean model are compared with finestructure estimates made from observations. A horizontal viscosity scheme restricted to only act on horizontally rotational modes (such as eddies) is introduced and tested. At lower resolutions with horizontal grid spacings of 2 km, the modeled IW dissipation from numerical model agrees reasonably well with observations in some cases when the restricted form of horizontal viscosity is used. This suggests the possibility that if restricted forms of horizontal viscosity are adopted by global models with similar resolutions, they could be used to diagnose and map IW dissipation distributions. At higher resolutions with horizontal grid spacings of ~250 m, the dissipation from vertical shear and horizontal viscosity act much more strongly resulting in dissipation overestimates; however, the vertical-shear dissipation itself is found to agree well with observations.

Plain Language Summary Oceanic mixing impacts circulation, stratification (layering by density), and the uptake and transport of heat and nutrients. Over most of the ocean, mixing is caused by the breaking (turnover) of internal waves lying on the interfaces of density layers. Most ocean models do not contain a resolved internal wavefield, and therefore must parameterize internal wave (IW) mixing based upon external information. Recently developed high-resolution ocean models with credible representations of internal waves may make it possible to map and understand global IW mixing without use of external information. Here we compare vertical profiles (profiles in depth) of IW dissipation in a regional model, which can be used to understand sensitivities to numerical schemes and grid spacings. With grid spacings that are attainable in global models, modeled dissipation profiles lie somewhat close to observed profiles, as long as certain choices are made within the numerical schemes. One numerical dissipation scheme is designed to realistically remove energy from eddy fields, which are the non-wavelike motions in the ocean, and we have adapted this scheme to act less strongly on internal waves. Using this modified scheme, we find that high-resolution global models may already be able to map IW dissipation.

Key Points:

- Vertical profiles of internal wave (IW) dissipation in high-resolution regional ocean simulations are compared with observed profiles
- Profiles in runs with a restricted form of horizontal viscosity and resolutions attainable in global models are close to observations
- Results suggest high-resolution global models can be used to map IW dissipation after numerical sensitivities are tested in regional models

Supporting Information:

Supporting Information may be found in the online version of this article.

Correspondence to:

J. Skitka,
Joseph.Skitka@gmail.com

Citation:

Skitka, J., Arbic, B. K., Ma, Y., Momeni, K., Pan, Y., Peltier, W. R., et al. (2024). Internal-wave dissipation mechanisms and vertical structure in a high-resolution regional ocean model. *Geophysical Research Letters*, *51*, e2023GL108039. https://doi.org/10.1029/2023GL108039

Received 30 JAN 2024
Accepted 10 JUL 2024

1. Introduction

For nearly 30 years, considerable effort has been put into correctly modeling eddy dissipation in ocean models with sufficient resolution to be eddy-permitting (Fox-Kemper et al., 2019; Griffies & Hallberg, 2000). This work has directly enabled advances in the ability of such models to find agreement with theory and observations of ocean turbulence (Bachman, 2019; Jansen et al., 2015; Pearson et al., 2017); it can also offer indirect improvements by shifting dissipation to other physically based operators, such as bottom drag (Arbic et al., 2009; Pearson et al., 2017), thereby improving the credibility of diagnosed eddy dissipation maps. The present state of high-resolution ocean modeling now similarly prompts the adaptation of dissipation mechanisms to account for the inclusion of an internal-wave (IW) spectral continuum, which has been documented in observations for decades (Garrett & Munk, 1972, 1975) but which has only recently been partially resolved in some global ocean models (Müller et al., 2015; Rocha et al., 2016; Savage et al., 2017; Solano et al., 2023). An added challenge to the closure of the IW continuum is the simultaneous handling of multiple cascade-like processes in a single simulation without compromising the handling of eddy closures. Does the coexistence of eddy and IW cascades prevent separate and accurate accounting of dissipation and diffusivities to close these cascades? The reward for

navigating these challenges could be accurately represented IW spectra in numerical models and, by extension, the ability to replicate and predict IW dissipation and mixing patterns in the ocean. Such mixing arising from dissipation of the IW continuum has a strong impact on oceanic stratification and circulation (Wunsch & Ferrari, 2004) as well as the uptake, storage, and transport of biologically important nutrients and heat (Whalen et al., 2020).

In the past decade, global ocean models that have frequently updated astronomical and wind forcing (Arbic, 2022; Arbic et al., 2010, 2018) have represented the larger-scale part of the IW continuum (Müller et al., 2015; Rocha et al., 2016; Savage et al., 2017), an important first step in resolving the IW cascade. These larger-scale IWs are mostly directly energized through wind-driven near-inertial motions, internal tides generated by tidal flow over topographic features, and nonlinear interactions between IWs and mesoscale eddies (MacKinnon et al., 2017; McComas, 1977; Skitka et al., 2024). Yet many of the cascade-like interactions of the IW continuum involve scales that are smaller than those resolved by global models. Regional models can be run with finer grid spacings, and are better able to resolve the nonlinear IW interactions (Nelson et al., 2020; Pan et al., 2020; Skitka et al., 2024; Thakur et al., 2022) that are thought to be important for accurately representing the empirical Garrett-Munk spectrum (Garrett & Munk, 1979) and its associated dissipation and mixing.

In IW-permitting ocean models, IW energy is dissipated through a combination of numerical mechanisms that are based on a physical picture of IW breaking (e.g., shear-based instabilities, Large et al., 1994, and flow over topography, Klymak & Legg, 2010), mechanisms that were formulated with eddy fields in mind (e.g., horizontal-viscosity Large Eddy Simulation, or LES, schemes, Fox-Kemper & Menemenlis, 2008; Smagorinsky, 1963), and mechanisms that are agnostic to the type of flow they are acting on (e.g., linear scalar harmonic viscosity). Previous work has shown that modification to these mechanisms can improve aspects of the IW continuum (Thakur et al., 2022). This paper evaluates the relative importance of the dissipation mechanisms described above for dissipating energy in a numerical model. We place special emphasis on investigating modifications to the horizontal viscosity scheme and consequent potential improvements to the modeled IW representation, particularly in the ocean interior as opposed to the near-surface and near-bottom processes.

Given the direct representation of IWs and some of their interactions in global and regional ocean models, we are in a position to compare IW dissipation and mixing with observations. Such model-observation comparisons could be used to evaluate the aforementioned potential of ocean models for predicting IW-induced dissipation and mixing patterns. Estimates of IW dissipation made with fine-structure observations have previously served as a basis for comparison with a parameterized model of the IW Garett-Munk spectrum, the IW, Dissipation, Energy, and Mixing (IDEMIX) model (Pollmann, 2020; Pollmann et al., 2017a). Comparison of observations with directly diagnosed IW dissipation as represented in a numerical model, however, remains unexplored. This paper will focus on comparisons with observations of IW dissipation made using a finescale parameterization (Gregg, 1989; Polzin et al., 1995, 2014). The connection to mixing and turbulent eddy diffusivity will be reserved for a subsequent paper.

2. Methods

2.1. Numerical Model

The numerical simulations are performed in a $6° \times 8°$ region north-east of Hawaii (Figure 1). This numerical domain has been the subject of several recent investigations (Nelson et al., 2020; Pan et al., 2020; Skitka et al., 2024; Thakur et al., 2022). The simulations are run with the MITgcm (Marshall et al., 1997) using rigidly imposed boundaries from a global-model run, as described in Nelson et al. (2020), but with a uniform vertical grid in the ocean interior, as described in Thakur et al. (2022). The boundary conditions account for remotely generated IWs, which are necessary to accurately represent the IW continuum (Mazloff et al., 2020; Nelson et al., 2020). "Low-resolution" will refer to the numerical simulations with 109 vertical levels and 2 km horizontal grid spacing, comparable to the grid spacings in the parent global simulation, the LLC4320 (Rocha et al., 2016), but with a maximum vertical grid spacing of 100 m. "High-resolution" will refer to simulations with 264 vertical levels and ∼250 m horizontal grid spacing, with a maximum vertical grid spacing of 25 m. Other grid details are described in Thakur et al. (2022). Our regional model and grid formulation permits a partial representation of the IW continuum, including some nonlinear IW dynamics (Nelson et al., 2020; Pan et al., 2020; Skitka et al., 2024). Specifically, the model obeys consistency relations of IWs (Nelson et al., 2020), has IW wavenumber and frequency KE spectra that approach the empirical Garrett-Munk Spectrum and observations (Nelson et al., 2020;

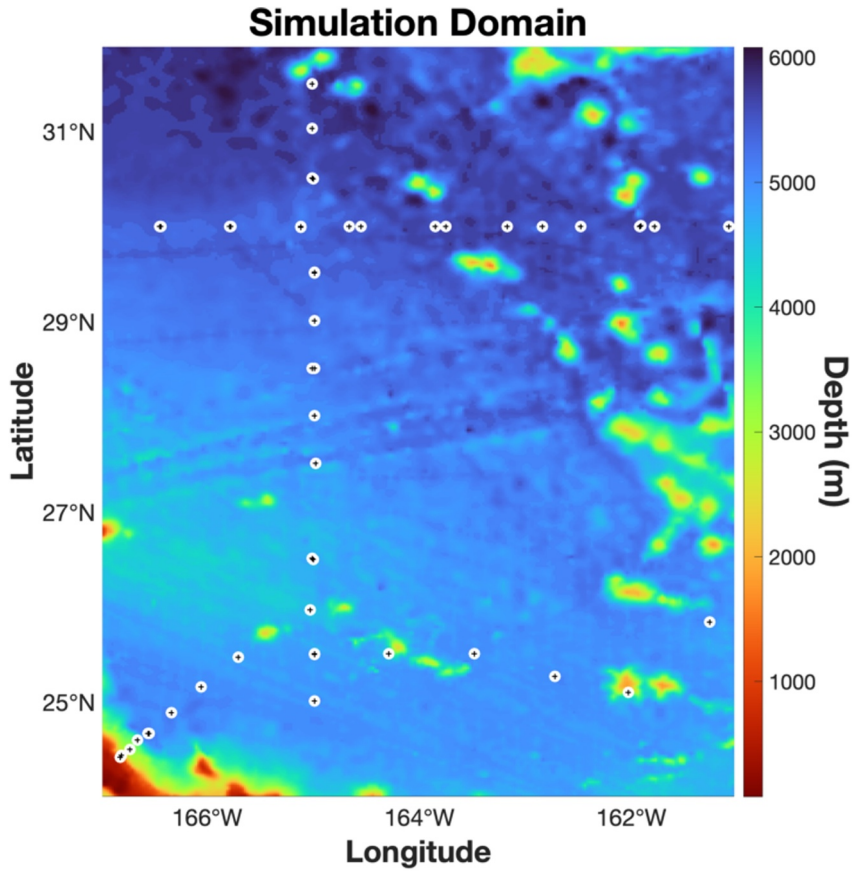

Figure 1. Bathymetry of the region of study, adapted from Skitka et al. (2024). Circles with a plus sign have been added to indicate the locations of CTD data from Kunze (2017).

Thakur et al., 2022), and represents at least some of the nonlinear interactions that shape the IW energy spectrum (Pan et al., 2020; Skitka et al., 2024). We have further provided comparisons of vertical profiles of eddy and IW KE in the supplemental information to this paper.

2.2. Numerical Dissipation Schemes

For a typical Garrett-Munk IW spectrum, Dematteis and Lvov (2023) found, based on their idealized calculations, that energy can be expected to dissipate into turbulence via the induced diffusion scattering mechanism mostly to the smallest vertical rather than horizontal scales (see their Figure 4). Accurate IW dissipation in a numerical model will likely reflect this (depending on the aspect ratio of its resolution), and a reasonable approach to closing the IW cascade would then be tailoring the vertical viscosity scheme to resemble the magnitude and mechanism of the instabilities that dissipate IW energy in the ocean, such as shear-induced mixing and dissipation (Large et al., 1994). In the low-resolution model formulation used here, the vertical shear mechanism (described in the supporting information), which is part of the κ-Profile Parameterization (KPP) (Large et al., 1994) and is triggered when a local vertical-gradient Richardson number threshold is met, does not dissipate a leading-order portion of the IW energy; rather, the horizontal LES viscosity and (if enabled) the background vertical viscosity do. The (vertical) Prandtl number for the background component of KPP in these simulations is inherited from the global LLC4320 model and is quite large, $\mathcal{O}(10^3)$, meaning momentum diffuses vertically much more rapidly than buoyancy and the shear-based viscosity is suppressed. The background vertical viscosity and diffusivity can simply be disabled in these runs, resulting in more accurate and energetic representation for high-vertical-wavenumber IWs (Thakur et al., 2022), while also enabling modeled shear instabilities to occur more frequently. However, we find that in such simulations with the background component disabled, most IW KE is

still primarily dissipated by the horizontal viscosity LES scheme, which is not designed to act in a physically correct manner on IWs.

Turning our attention instead to the role of the horizontal viscosity scheme in IW dissipation, we can assess whether it might be restricted or replaced with an IW-tailored scheme. As noted in the previous paragraph, we do this with the intention of eliminating spurious dissipation at high horizontal wavenumbers in favor of high vertical wavenumbers. In this numerical model, and in many others, a nonlinear LES is implemented to close the eddy cascade, and this LES necessarily acts on any IWs that are included in the model solution. The Leith LES scheme (Leith, 1996) used in our simulations is based on the modified form developed in Fox-Kemper and Menemenlis (2008). Reducing the overall strength of the Leith parameterization produces energy buildup in the regional simulations used for this paper. We can restrict the LES so that it selectively acts more strongly on eddy fields than on IWs. The complete separation of the flow into eddy and IW modes is computationally difficult. As an intermediate option, we note that much of the supertidal IW flow and very little of the eddy flow projects onto horizontally divergent modes. Many solvers, including the MITgcm (Adcroft et al., 2015), are implemented with vector-invariant forms of the momentum equations, which allow for the efficient restriction of viscosities to act on only rotational components. The velocity tendency resulting from the horizontal biharmonic Leith viscosity can be written:

$$\begin{aligned}\frac{\partial}{\partial t}(\mathbf{u})_{\text{h. visc.}} &= \nabla_h \cdot \left(\nu_{\text{h4L}} \nabla_h \left(\nabla^2 \mathbf{u}\right)\right) \\ &= \underbrace{\nabla_h \left(\nu_{\text{h4L}} \nabla_h \cdot \left(\nabla^2 \mathbf{u}\right)\right)}_{\text{acts on } \mathbf{u}_{div}} - \underbrace{\nabla \times \left(\nu_{\text{h4L}} \left(\nabla \times \left(\nabla^2 \mathbf{u}\right)\right)_z \hat{\mathbf{z}}\right)}_{\text{acts on } \mathbf{u}_{rot}} + C\end{aligned} \tag{1}$$

where $\mathbf{u} = (u, v, 0)$ is the 3D horizontal velocity vector, $\nabla_h \cdot$ is the horizontal divergence operator, ∇_h is the horizontal gradient operator, a z subscript indicates the z-component of a vector, C is a correction term containing the effects of nonuniform viscous coefficients and is given in the Supporting Information S1, ν_{h4L} is the horizontal biharmonic Leith viscosity (Fox-Kemper & Menemenlis, 2008) (defined below), and $\mathbf{u}_{rot/div}$ refer to any decomposition $\mathbf{u} = \mathbf{u}_{rot} + \mathbf{u}_{div}$ such that $\nabla_h \cdot \mathbf{u}_{rot} = 0$ and $(\nabla \times \mathbf{u}_{div})_z = 0$. While we compute horizontal viscosity using the biharmonic Leith scheme, this form is also applicable to other biharmonic and harmonic forms of the horizontal viscosity. A restricted viscous dissipation that acts substantially less on IWs can be obtained by omitting the divergent and correction terms in Equation 1:

$$\frac{\partial}{\partial t}(\mathbf{u})_{\text{h. visc. div off}} = -\nabla \times \left(\nu_{\text{h4L}} \nabla \times \left(\nabla^2 \mathbf{u}\right)\right). \tag{2}$$

IWs are purely horizontally divergent in the limit of high frequency and equal parts divergent and rotational in the limit of low frequencies (Gill, 1982), so the Leith scheme in Equation 2 can still act on IWs, but preferentially at lower frequencies.

The nonlinear viscous coefficient, ν_{h4L}, can itself be modified to change its response to horizontally divergent modes. From Fox-Kemper and Menemenlis (2008):

$$\nu_{\text{h4L}}(\Lambda, \Lambda_d) = \left(\frac{\Delta x}{\pi}\right)^6 \sqrt{\Lambda^{12} \left|\nabla_h^2 (\nabla \times \mathbf{u})_z\right|^2 + \Lambda_d^{12} \left|\nabla_h^2 (\nabla_h \cdot \mathbf{u})\right|^2}. \tag{3}$$

Here, ∇_h^2 is the Laplacian computed with only the horizontal components, Δx is the horizontal grid spacing, and Λ, Λ_d are dimensionless parameters. The term that includes Λ_d was introduced by Fox-Kemper and Menemenlis (2008) in order to stabilize horizontal-grid-scale energy buildup that occurred in global ocean simulations using this damping scheme.

In order to investigate the relative impact of changing Λ_d versus using Equation 2 instead of Equation 1, we look to their Courant–Friedrichs–Lewy (CFL) (Courant et al., 1967) parameters,

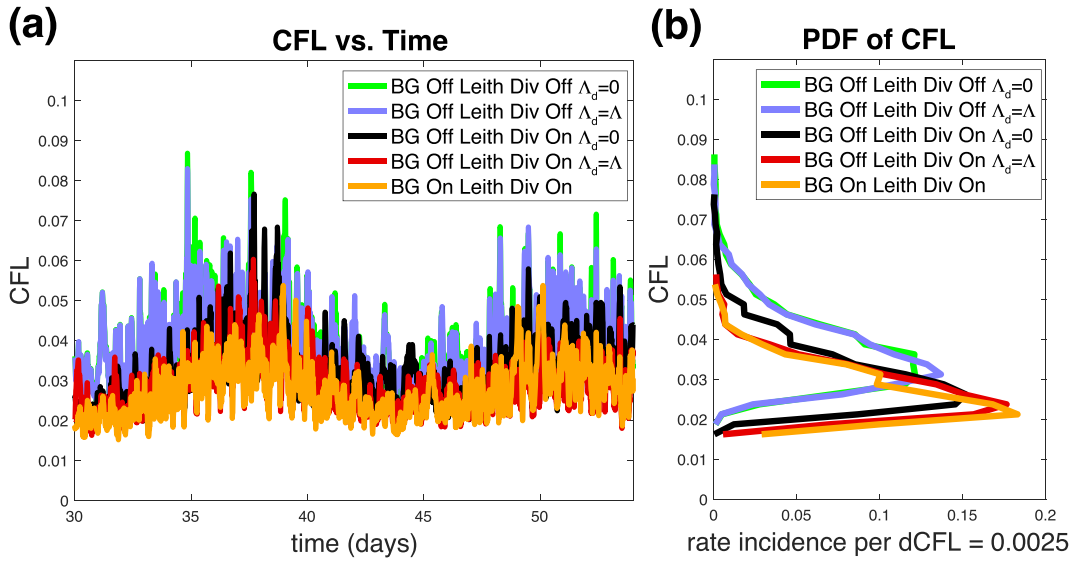

Figure 2. The CFL parameter (Equation 4) as a function of time (panel a) and as a probability distribution function (panel b) for various low-resolution runs with different dissipation schemes described in the text. Here, BG refers to whether the KPP background vertical viscosity and diffusivity. "Leith Div Off" refers to a simulation in which Leith eddy viscosity (as described in Fox-Kemper & Menemenlis, 2008) is constrained to not act on horizontally divergent modes (Equation 2), while $\Lambda_d = \Lambda$ refers to a simulation that uses the modified form of the Leith viscosity that responds to horizontally divergent motions in the flow (Fox-Kemper & Menemenlis, 2008) but doesn't necessarily act on the horizontally divergent modes in the flow (Equation 3).

$$\mathrm{CFL} = \max\left(\sqrt{\left(\frac{u\Delta t}{\Delta x}\right)^2 + \left(\frac{v\Delta t}{\Delta y}\right)^2 + \left(\frac{w\Delta t}{\Delta z}\right)^2}\right), \tag{4}$$

where u, v, w are the x, y, and z components of velocity, Δx, Δy, and Δz are the components of the grid spacing, Δt is the timestep, and max() refers to a maximum in the domain at a given time. The CFL parameter is a measure of peak nondimensional velocity in the domain; the timestep must be chosen such that $\mathrm{CFL} \lesssim \mathcal{O}(1)$ in order to be stable. Figure 2 shows the CFL parameter of low-resolution simulations with and without the Leith scheme applied to the horizontally divergent modes (Equations 1 and 2, respectively), as well as with $\Lambda_d = \Lambda = 2.15$ and $\Lambda_d = 0$. Unlike in Fox-Kemper and Menemenlis (2008), we found in these model runs, which have about 10× the resolution, that toggling Λ_d has only a small effect on the flow solution compared to restricting the Leith viscosity to only act on the rotational modes (Figure 2). This paper tests the version of Leith that acts on rotational modes only, as in Equation 2, and with $\Lambda_d = 0$, which is labeled as "Leith (Div. Off)" throughout the paper. Finally, the magnitude of the CFL parameter (Figure 2) suggests that the divergence-restricted Leith scheme can be implemented in a numerical model with only modest restrictions on the timestep.

2.3. Observations and Dissipation Calculations

Exact temporal and spatial alignment of the observational data with numerical model output cannot be readily achieved given the availability of observations and the computational cost associated with analyzing data. The question that this paper addresses is: can the numerical model output capture in an approximate sense the scale and general trends of the dissipation observations?

Pollmann et al. (2017a) (PEO17) used a finescale parameterization (Kunze et al., 2006; Polzin et al., 1995) to estimate global dissipation rates from Argo float data (https://www.argo.ucsd.edu) averaged over a 15-year period, from 2006 to 2015. These estimates were used by PEO17 to make global maps of IW dissipation as a basis of comparison with IDEMIX. For this paper, we use the PEO17 estimates presented at depth-ranges of 100 m resolution from 200 m depth to 1,800 m depth (Pollmann et al., 2017b). The PEO17 estimates are averaged over bins with a horizontal grid spacing of 1.5° × 1.5°. Below 500 m, this data set is sparse, defined for 15%–35%

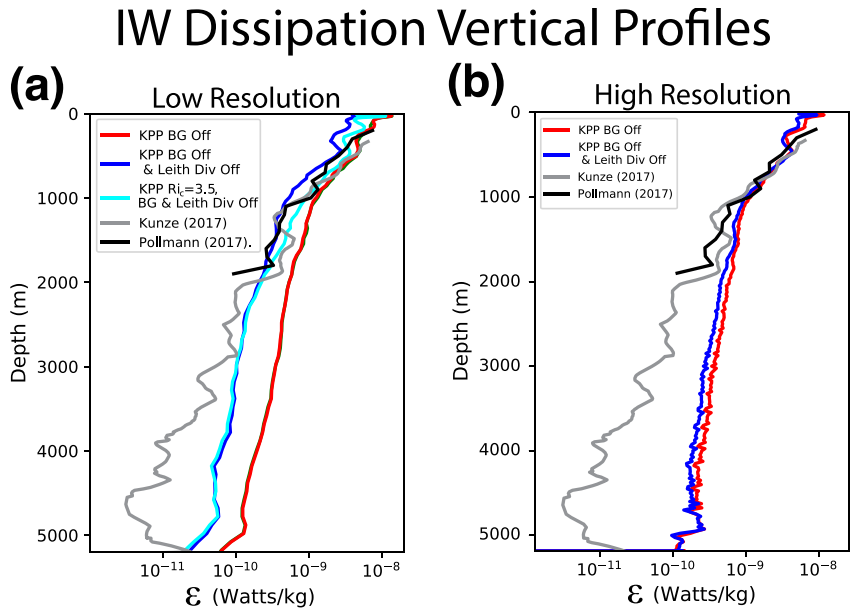

Figure 3. Vertical dissipation profiles (Equation 5) from simulations with different dissipation mechanisms enabled for the "low resolution" cases (Panel a), and for the high resolution cases (Panel b) compared with dissipation profiles estimated with finescale parameterizations (Kunze et al., 2006; Polzin et al., 2014) using Argo floats (PEO17; Pollmann et al., 2017a) and dropped CTD profiles (K17; Kunze, 2017).

of bins at a given depth. In order to get a statistically representative estimate of the dissipation in this region, it is necessary to average PEO17's dissipation over a wider region than the simulation domain (161°W–167°W by 24°N–32°N); an extra 3.5° buffer is used on all sides.

Kunze (2017) (K17) applied a finescale parameterization to ship-based CTD data. Of the approximately 13,000 casts made in the Pacific Ocean, 50 were made within the computational domain studied in this paper; the locations of these are displayed in Figure 1. The casts occur along ship tracks that span the domain, some very close to one another. The resulting profiles cover much of the water column, generally extending to about 1,000 m above the ocean floor.

The simulations used in this paper were run for 60 days, beginning on 1 March 2012. IW dissipation is diagnosed from the final week of numerical output (to allow for spinup), corresponding to 22 April–28 April 2012. Details of the numerical methods used to diagnose particular dissipation mechanisms are given in Appendix A5 of Skitka et al. (2024). A high-pass filter retaining only frequencies greater than $0.8f_0$, where $f_0 = 6.85 \times 10^{-5}$ rad/s, is used to isolate internal gravity waves, including tides, near-inertial waves, and the internal gravity-wave continuum. Note that this Eulerian filter has the shortcoming that bottom-generated Lee waves are included in the "eddy" component. The IW dissipation associated with a given dissipation mechanism can then be computed as

$$\varepsilon_{\mathrm{IW}} = -\left\langle \mathbf{u}^{\mathrm{IW}} \cdot \partial_t(\mathbf{u})_{\mathrm{term}} \right\rangle, \tag{5}$$

where $\mathbf{u}^{\mathrm{IW}}$ is the IW velocity field defined with the high-pass filter, $\partial_t(\mathbf{u})_{\mathrm{term}}$ refers to the velocity tendency resulting from a dissipative term, such as in Equation 1, and the angle brackets indicate averaging over horizontal spatial dimensions and time. Because the data products of both PEO17 and K17 do not extend to the ocean floor, bottom drag is explicitly omitted from diagnosed dissipation calculations. The observational profiles also do not extend to within 200 m of the sea surface, so the mixed-layer dissipation scheme, which mostly acts within the upper 100 m, is also omitted.

3. Results

Vertical profiles of IW dissipation from numerical model output and the observation-based PEO17 and K17 estimates (Figure 3) indicate that PEO17 and K17 are in reasonable agreement with one another over the depths at

which both are defined, lending confidence to these products as a basis of comparison with numerical model output. At low resolutions, the numerically modeled IW dissipation overestimates the observations below 2,000 m if the conventional form of Leith viscosity is used (Figure 3a). However the modeled dissipation is closer to both sets of observations below 2,000 m if the divergent part of the Leith viscosity is disabled. In the latter cases, the model dissipation still overshoots observations between about 3,600 and 5,000 m but agrees more closely between 5,000 and 5,200 m. Whether KPP background vertical viscosity is enabled or disabled does not have much of an impact on the profiles and so "KPP BG Off, Leith Div. On" is not shown. The "Leith Div Off" case undershoots the observations by less than an order of magnitude in the top 500 m; this can be adjusted to a more accurate level of dissipation by increasing the sensitivity of the shear dissipation (KPP Off, Leith Div. Off, and $Ri_c = 3.5$ in Figure 3a).

Figure 4 displays decompositions of the dissipation profiles into their component mechanisms (see Section 2.2) for the KPP-BG-off and Leith-Div-off, high-resolution all-on, and low-resolution all-on cases, respectively. Figures 4a and 4b show the decomposition for KPP-BG-off and Leith-Div-on, which has largely the same trends as in the all-on case in Figures 4c and 4d. Figures 4c and 4d indicate that KPP BG is not a leading-order dissipation mechanism below 1,000 m depth in either low- or high-resolution cases and is comparable to Leith in the top 1,000 m. This helps explain why disabling KPP BG does not significantly impact the overall dissipation profiles yet still can increase the energy of the relatively low-energy highest vertical wavenumbers (Thakur et al., 2022). The other vertical viscosity is the nonlinear KPP shear mechanism, and its associated dissipation is smaller than that of the Leith horizontal viscosity in all cases and resolutions below 1,000 m depth. The vertical wavenumber spectrum of IWs is not predominantly damped by vertical viscosity. The unrestricted version of Leith horizontal viscosity scheme is acting at leading order at all depths in all simulations.

Why does the KPP-BG-off/Leith-div.-off case agree with observations more closely in the low-resolution case than in the high-resolution case? Below 1,000 m, the KPP shear-based dissipation is at least an order of magnitude smaller in low-resolution cases than in high-resolution cases. It may be useful to think of the KPP-shear term as resolution-restricted in the low-resolution case; its effective disabling allows the rotational part of the Leith scheme in the "Leith-div.-off" case to better agree with observations. Figures 4c and 4d also show that the divergent part of the Leith dissipation is larger relative to the rotational part below depths of 1,500 m, possibly reflecting a smaller portion of near-inertial waves in the ocean interior. Disabling the divergent part of the Leith viscosity therefore particularly reduces the profiles below 1,500 m, where the model typically overshoots the observed rates of dissipation. An analysis of spatial variance in these profiles suggests general overlap between low-resolution model output and observations except between 3,600 and 4,900 m depth (see Supporting Information S1) These results are consistent with the KPP-BG-off, Leith-div.-off case potentially being a good diagnostic of ocean interior IW dissipation at 2 km horizontal and 100 m vertical resolutions, which are accessible in global models.

In the high-resolution cases (~250 m horizontal and 25 m vertical resolutions), the dissipation of the Leith scheme acting on horizontally rotational modes is larger than in the low-resolution cases. It could be that the horizontal viscosity scheme is dissipating a larger portion of KE at this high resolution because the model represents a greater prevalence of spectrally local interactions that rapidly transfer energy to high horizontal wavenumbers (Dematteis et al., 2022). The resulting total dissipation is larger than in observations, even when the Leith dissipation is restricted. In the high-resolution cases with the KPP BG disabled, the shear-based dissipation itself is in agreement with the observations at most depths below the upper 500 m. In cases with all dissipation mechanisms enabled, the KPP BG dissipation is similarly in rough agreement with observations below 500 m depth.

4. Discussion

We have shown that vertical profiles of IW dissipation in our regional simulations are reasonably similar to profiles in observations, provided some considerations pertaining to the numerical dissipation mechanisms are taken into account. Our results point toward a future in which IW dissipation and mixing will in part arise naturally from simulations, and evolve naturally as climate changes, rather than arising from parameterizations that draw upon information external to the model runs themselves.

An exciting prospect based on these results is that for global models at 2 km resolutions and 109 vertical levels, horizontal dissipation schemes can be restricted to not act on horizontally divergent modes and the IW dissipation

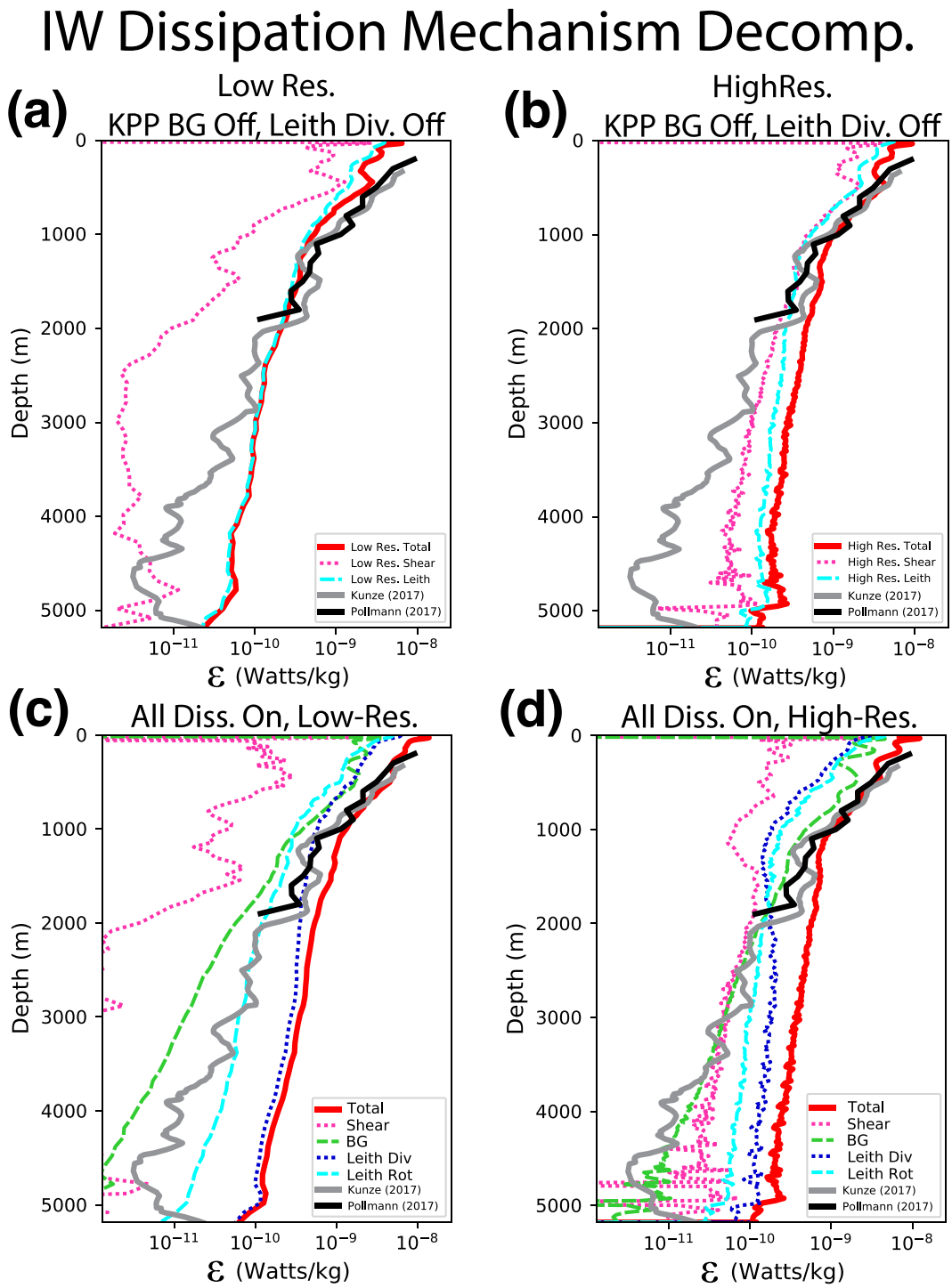

Figure 4. Vertical profiles of decompositions of internal wave dissipation for specific cases.

can be diagnosed as a function of space, time, and depths, especially below 500 m. Near-surface dissipation appears sensitive to vertical viscosity schemes that will be studied in an upcoming paper. The CFL constraints of such a modification are modest (see Section 2.2), and the resulting improvements to the IW field may have unanticipated benefits for other flow features including the large-scale circulation. Further studies of different regions and seasons are needed to confirm that the agreement between model and observed results shown here is not random and whether other dissipation terms need to be included. We believe it is highly suggestive that

dissipation results from multiple observations collected using different methods and from numerical simulations generally overlap within uncertainties.

At very high resolutions (250 m horizontal, 256 vertical levels) at which the KPP-shear mechanism is fully activated, the Leith dissipation is larger than the observed IW dissipation, which KPP-shear adequately captures. These results suggest that the prognostic dynamics associated with IWs would be more accurate if the Leith dissipation were further restricted to act much more weakly, or not at all, on IWs. There is an opening here for the development of either a new IW-tailored LES-type simulation or for more effective use of KPP-shear dissipation as an IW closure if Leith viscosity is further restricted. Finding ways to efficiently further restrict horizontal viscosity schemes is therefore a priority and would help to address the fundamental question of whether the eddy and IW cascades can be simultaneously closed with a common numerical dissipation scheme.

Data Availability Statement

The numerical results presented in this paper, processing code used to generate these results, as well as source code used to generate raw data are available at Skitka (2023). Finestructure-based observational data from PEO17 is archived at Pollmann et al. (2017b) while K17 is available at https://ftp.nwra.com/outgoing/kunze/iwturb/.

Acknowledgments
We thank Friederike Pollmann for sharing and explaining observational data in an approachable format. We also thank Matthew Alford, Eric Kunze, Jennifer MacKinnon, Carl Wunsch, Roy Barkan, and Kurt Polzin for many useful discussions on IW dynamics and dissipation over the years. We thank the two anonymous reviewers. JS and BKA acknowledge support from Office of Naval Research Grant N00014-19-1-2712. RT and BKA acknowledge support from National Science Foundation Grants OCE-1851164 and OCE-2319142 and NASA Grant 80NSSCK1135. WRP was supported by the Natural Sciences and Engineering Research Council of Canada under the NSERC Discovery Grant A9627. DM carried out research at JPL, Caltech, under contract with NASA, with support from the Physical Oceanography and Modeling, Analysis, and Prediction Programs. All simulations in this study were performed on the Niagara supercomputer of the SciNet facility of the University of Toronto, which is a component of the Digital Research Alliance of Canada. YP acknowledges NSF OCE2241495.

References

Adcroft, A., Campin, J.-M., Dutkiewicz, S., Evangelinos, C., Ferreira, D., Forget, G., et al. (2015). *MITgcm user's manual*. MIT department of EAPS.

Arbic, B. K. (2022). Incorporating tides and internal gravity waves within global ocean general circulation models: A review. *Progress in Oceanography*, *206*, 102824. https://doi.org/10.1016/j.pocean.2022.102824

Arbic, B. K., Alford, M. H., Ansong, J. K., Buijsman, M. C., Ciotti, R. B., Farrar, J. T., et al. (2018). A primer on global internal tide and internal gravity wave continuum modeling in HYCOM and MITgcm. In E. Chassignet, A. Pascual, J. Tintore, & J. Verron (Eds.), *New frontiers in operational oceanography* (pp. 307–392). GODAE OceanView. https://doi.org/10.17125/gov2018.ch13

Arbic, B. K., Shriver, J. F., Hogan, P. J., Hurlburt, H. E., McClean, J. L., Metzger, E. J., et al. (2009). Estimates of bottom flows and bottom boundary layer dissipation of the oceanic general circulation from global high-resolution models. *Journal of Geophysical Research*, *114*(C2), C02024. https://doi.org/10.1029/2008JC005072

Arbic, B. K., Wallcraft, A. J., & Metzger, E. J. (2010). Concurrent simulation of the eddying general circulation and tides in a global ocean model. *Ocean Modelling*, *32*(3–4), 175–187. https://doi.org/10.1016/j.ocemod.2010.01.007

Bachman, S. D. (2019). The GM+ E closure: A framework for coupling backscatter with the Gent and McWilliams parameterization. *Ocean Modelling*, *136*, 85–106. https://doi.org/10.1016/j.ocemod.2019.02.006

Courant, R., Friedrichs, K., & Lewy, H. (1967). On the partial difference equations of mathematical physics. *IBM Journal of Research and Development*, *11*(2), 215–234. https://doi.org/10.1147/rd.112.0215

Dematteis, G., & Lvov, Y. V. (2023). The structure of energy fluxes in wave turbulence. *Journal of Fluid Mechanics*, *954*, A30. https://doi.org/10.1017/jfm.2022.995

Dematteis, G., Polzin, K., & Lvov, Y. V. (2022). On the origins of the oceanic ultraviolet catastrophe. *Journal of Physical Oceanography*, *52*(4), 597–616. https://doi.org/10.1175/jpo-d-21-0121.1

Fox-Kemper, B., Adcroft, A., Böning, C. W., Chassignet, E. P., Curchitser, E., Danabasoglu, G., et al. (2019). Challenges and prospects in ocean circulation models. *Frontiers in Marine Science*, *6*, 65. https://doi.org/10.3389/fmars.2019.00065

Fox-Kemper, B., & Menemenlis, D. (2008). Can large eddy simulation techniques improve mesoscale rich ocean models? In *American Geophysical Union Geophysical Monograph Series* (Vol. 177, pp. 319–337). https://doi.org/10.1029/177gm19

Garrett, C., & Munk, W. (1972). Space-time scales of internal waves. *Geophysical Fluid Dynamics*, *3*(3), 225–264. https://doi.org/10.1080/03091927208236082

Garrett, C., & Munk, W. (1975). Space-time scales of internal waves: A progress report. *Journal of Geophysical Research*, *80*(3), 291–297. https://doi.org/10.1029/jc080i003p00291

Garrett, C., & Munk, W. (1979). Internal waves in the ocean. *Annual Review of Fluid Mechanics*, *11*(1), 339–369. https://doi.org/10.1146/annurev.fl.11.010179.002011

Gill, A. E. (1982). *Atmosphere-ocean dynamics* (Vol. 30). Academic press.

Gregg, M. C. (1989). Scaling turbulent dissipation in the thermocline. *Journal of Geophysical Research*, *94*(C7), 9686–9698. https://doi.org/10.1029/jc094ic07p09686

Griffies, S. M., & Hallberg, R. W. (2000). Biharmonic friction with a Smagorinsky-like viscosity for use in large-scale eddy-permitting ocean models. *Monthly Weather Review*, *128*(8), 2935–2946. https://doi.org/10.1175/1520-0493(2000)128<2935:bfwasl>2.0.co;2

Jansen, M. F., Held, I. M., Adcroft, A., & Hallberg, R. (2015). Energy budget-based backscatter in an eddy permitting primitive equation model. *Ocean Modelling*, *94*, 15–26. https://doi.org/10.1016/j.ocemod.2015.07.015

Klymak, J. M., & Legg, S. M. (2010). A simple mixing scheme for models that resolve breaking internal waves. *Ocean Modelling*, *33*(3–4), 224–234. https://doi.org/10.1016/j.ocemod.2010.02.005

Kunze, E. (2017). Internal-wave-driven mixing: Global geography and budgets. *Journal of Physical Oceanography*, *47*(6), 1325–1345. https://doi.org/10.1175/jpo-d-16-0141.1

Kunze, E., Firing, E., Hummon, J. M., Chereskin, T. K., & Thurnherr, A. M. (2006). Global abyssal mixing inferred from lowered ADCP shear and CTD strain profiles. *Journal of Physical Oceanography*, *36*(8), 1553–1576. https://doi.org/10.1175/jpo2926.1

Large, W. G., McWilliams, J. C., & Doney, S. C. (1994). Oceanic vertical mixing: A review and a model with a nonlocal boundary layer parameterization. *Reviews of Geophysics*, *32*(4), 363–403. https://doi.org/10.1029/94rg01872

Leith, C. (1996). Stochastic models of chaotic systems. *Physica D: Nonlinear Phenomena*, *98*(2–4), 481–491. https://doi.org/10.1016/0167-2789(96)00107-8

MacKinnon, J. A., Zhao, Z., Whalen, C. B., Waterhouse, A. F., Trossman, D. S., Sun, O. M., et al. (2017). Climate process team on internal wave–driven ocean mixing. *Bulletin of the American Meteorological Society*, *98*(11), 2429–2454. https://doi.org/10.1175/bams-d-16-0030.1

Marshall, J., Hill, C., Perelman, L., & Adcroft, A. (1997). Hydrostatic, quasi-hydrostatic, and nonhydrostatic ocean modeling. *Journal of Geophysical Research*, *102*(C3), 5733–5752. https://doi.org/10.1029/96jc02776

Mazloff, M. R., Cornuelle, B., Gille, S. T., & Wang, J. (2020). The importance of remote forcing for regional modeling of internal waves. *Journal of Geophysical Research: Oceans*, *125*(2), e2019JC015623. https://doi.org/10.1029/2019jc015623

McComas, C. (1977). Equilibrium mechanisms within the oceanic internal wave field. *Journal of Physical Oceanography*, *7*(6), 836–845. https://doi.org/10.1175/1520-0485(1977)007<0836:emwtoi>2.0.co;2

Müller, M., Arbic, B. K., Richman, J. G., Shriver, J. F., Kunze, E. L., Scott, R. B., et al. (2015). Toward an internal gravity wave spectrum in global ocean models. *Geophysical Research Letters*, *42*(9), 3474–3481. https://doi.org/10.1002/2015gl063365

Nelson, A., Arbic, B., Menemenlis, D., Peltier, W., Alford, M., Grisouard, N., & Klymak, J. (2020). Improved internal wave spectral continuum in a regional ocean model. *Journal of Geophysical Research: Oceans*, *125*(5), e2019JC015974. https://doi.org/10.1029/2019jc015974

Pan, Y., Arbic, B. K., Nelson, A. D., Menemenlis, D., Peltier, W., Xu, W., & Li, Y. (2020). Numerical investigation of mechanisms underlying oceanic internal gravity wave power-law spectra. *Journal of Physical Oceanography*, *50*(9), 2713–2733. https://doi.org/10.1175/jpo-d-20-0039.1

Pearson, B., Fox-Kemper, B., Bachman, S., & Bryan, F. (2017). Evaluation of scale-aware subgrid mesoscale eddy models in a global eddy-rich model. *Ocean Modelling*, *115*, 42–58. https://doi.org/10.1016/j.ocemod.2017.05.007

Pollmann, F. (2020). Global characterization of the ocean's internal wave spectrum. *Journal of Physical Oceanography*, *50*(7), 1871–1891. https://doi.org/10.1175/jpo-d-19-0185.1

Pollmann, F., Eden, C., & Olbers, D. (2017a). Evaluating the global internal wave model IDEMIX using finestructure methods. *Journal of Physical Oceanography*, *47*(9), 2267–2289. https://doi.org/10.1175/jpo-d-16-0204.1

Pollmann, F., Eden, C., & Olbers, D. (2017b). Wave-induced mixing from finescale parameterization applied to Argo float data (2006-2015) [Dataset]. https://doi.org/10.17882/97975

Polzin, K. L., Garabato, A. C. N., Huussen, T. N., Sloyan, B. M., & Waterman, S. (2014). Finescale parameterizations of turbulent dissipation. *Journal of Geophysical Research: Oceans*, *119*(2), 1383–1419. https://doi.org/10.1002/2013jc008979

Polzin, K. L., Toole, J. M., & Schmitt, R. W. (1995). Finescale parameterizations of turbulent dissipation. *Journal of Physical Oceanography*, *25*(3), 306–328. https://doi.org/10.1175/1520-0485(1995)025<0306:fpotd>2.0.co;2

Rocha, C. B., Gille, S. T., Chereskin, T. K., & Menemenlis, D. (2016). Seasonality of submesoscale dynamics in the Kuroshio Extension. *Geophysical Research Letters*, *43*(21), 11–304. https://doi.org/10.1002/2016gl071349

Savage, A. C., Arbic, B. K., Alford, M. H., Ansong, J. K., Farrar, J. T., Menemenlis, D., et al. (2017). Spectral decomposition of internal gravity wave sea surface height in global models. *Journal of Geophysical Research: Oceans*, *122*(10), 7803–7821. https://doi.org/10.1002/2017jc013009

Skitka, J. (2023). Data repository for internal-wave dissipation mechanisms and vertical structure in a high-resolution regional ocean model [dataset]. *Harvard Dataverse*. https://doi.org/10.7910/DVN/SXMJMQ

Skitka, J., Arbic, B. K., Thakur, R., Menemenlis, D., Peltier, W. R., Pan, Y., et al. (2024). Probing the nonlinear interactions of supertidal internal waves using a high-resolution regional ocean model. *Journal of Physical Oceanography*, *54*(2), 399–425. https://doi.org/10.1175/JPO-D-22-0236.1

Smagorinsky, J. (1963). General circulation experiments with the primitive equations: I. The basic experiment. *Monthly Weather Review*, *91*(3), 99–164. https://doi.org/10.1175/1520-0493(1963)091<0099:gcewtp>2.3.co;2

Solano, M. S., Buijsman, M. C., Shriver, J. F., Magalhaes, J., da Silva, J., Jackson, C., et al. (2023). Nonlinear internal tides in a realistically forced global ocean simulation. *Journal of Geophysical Research: Oceans*, *128*(12), e2023JC019913. https://doi.org/10.1029/2023jc019913

Thakur, R., Arbic, B. K., Menemenlis, D., Momeni, K., Pan, Y., Peltier, W. R., et al. (2022). Impact of vertical mixing parameterizations on internal gravity wave spectra in regional ocean models. *Geophysical Research Letters*, *49*(16), e2022GL099614. https://doi.org/10.1029/2022gl099614

Whalen, C. B., De Lavergne, C., Naveira Garabato, A. C., Klymak, J. M., MacKinnon, J. A., & Sheen, K. L. (2020). Internal wave-driven mixing: Governing processes and consequences for climate. *Nature Reviews Earth & Environment*, *1*(11), 606–621. https://doi.org/10.1038/s43017-020-0097-z

Wunsch, C., & Ferrari, R. (2004). Vertical mixing, energy, and the general circulation of the oceans. *Annual Review of Fluid Mechanics*, *36*(1), 281–314. https://doi.org/10.1146/annurev.fluid.36.050802.122121